

H α EMISSION FROM ACTIVE EQUAL-MASS, WIDE M DWARF BINARIES[†]HEATHER C. GUNNING^{1,2}, SARAH J. SCHMIDT^{1,3}, JAMES R. A. DAVENPORT¹, SAURAV DHITAL^{4,5}, SUZANNE L. HAWLEY¹,
ANDREW A. WEST⁵*Draft version July 7, 2021*

ABSTRACT

We identify a sample of near-equal mass wide binary M dwarf systems from the SLoWPoKES catalog of common proper-motion binaries and obtain follow-up observations of their chromospheric activity as measured by the H α emission line. We present optical spectra for both components of 48 candidate M dwarf binaries, confirming their mid-M spectral types. Of those 48 coeval pairs, we find eight with H α emission from both components, three with weak emission in one component and no emission in the other, and 37 with two inactive components. We find that of the eleven pairs with at least one active component, only three follow the net trend of decreasing activity strength ($L_{\text{H}\alpha}/L_{\text{bol}}$) with later spectral type. The difference in quiescent activity strength between the A and B components is larger than what would be expected based on the small differences in color (mass). For five binaries with two active components, we present 47 hours of time-resolved spectroscopy, observed on the ARC 3.5-m over twelve different nights. For four of the five pairs, the slightly redder (B) component exhibits a higher level of H α emission during the majority of the observations and the redder objects are the only components to flare. The full range of H α emission observed on these variable mid-M dwarfs is comparable to the scatter in H α emission found in single-epoch surveys of mid-M dwarfs, indicating that variability could be a major factor in the spread of observed activity strengths. We also find that variability is independent of both activity strength and spectral type.

Subject headings: stars

1. INTRODUCTION

M dwarfs are well known for harboring surface magnetic fields as strong as several kG (e.g., Johns-Krull & Valenti 1996; Valenti & Johns-Krull 2001), persisting on both sides of the fully convective boundary (\sim M4; Chabrier & Baraffe 1997). The strength of the magnetic fields in M dwarfs may be intrinsically tied to stellar rotation (on both sides of the convective boundary; Dobler et al. 2006; Browning et al. 2006), which has in turn been shown to depend on both mass and age (Irwin et al. 2011). These magnetic fields result in chromospheric heating, often observed through the presence and strength of H α emission (e.g., Hawley et al. 1996).

The presence of H α emission has been observed to depend on both mass (or its proxy, spectral type) and age: early-M dwarfs are active for a much shorter time (\sim 1 Gyr) than the mid- (\sim 4–6 Gyr) and late-M dwarfs ($>$ 7 Gyr; West et al. 2008). Chromospheric activity strength (usually quantified by the ratio of the luminosity of H α to the bolometric luminosity, $L_{\text{H}\alpha}/L_{\text{bol}}$) is also

related both to spectral type and age. $L_{\text{H}\alpha}/L_{\text{bol}}$ is relatively constant for M0–M4 dwarfs, then declines with later spectral type through M9 (West et al. 2004, 2011). The activity trends exhibit significant scatter compared to their dynamic range and measurement errors. Since the West et al. studies were based on an ensemble of single-epoch measurements, the observed spread in activity could originate from the intrinsic variability of the H α emission line, or could reflect some intrinsic range in magnetic activity strength.

Repeat observations of H α emission in M dwarfs often show variability (e.g., Bopp & Schmitz 1978), but it has only recently been investigated over both long and short timescales. On timescales of hours to months, \sim 80% of active M dwarfs show significant variability (Lee et al. 2010; Kruse et al. 2010), usually varying by factors of 1.25–4 in H α EW. In data averaged over 150 day windows, Gomes da Silva et al. (2011) found variability on 5–10 year timescales in 10 out of 30 M0–M5 dwarfs. These variability timescales could be linked to stellar rotation, the formation and dissipation of active regions, or long-term variations of the magnetic field. The relationships between H α variability, stellar mass, and age have not been thoroughly investigated. Bell et al. (2012), for example, found no net trend in H α variability as a function of spectral type, and an increase in variability with declining activity strength.

It is unknown how the broad trends in activity strength with respect to mass and age translate to individual systems, and whether the scatter in the observed trends is due to H α variability or is intrinsic to the M dwarf magnetic field strengths. To probe M dwarf activity strength and variability while controlling for mass and age, we have chosen to monitor a sample of near-equal mass, wide

schmidt@astronomy.ohio-state.edu

¹ Astronomy Department, Box 351580, University of Washington, Seattle, WA 98195, USA² Space Telescope Science Institute, Box 351580, 3700 San Martin Drive, Baltimore, MD 21218, USA³ Department of Astronomy, Ohio State University, 140 West 18th Avenue, Columbus, OH 43210, USA⁴ Department of Physical Sciences, Embry-Riddle Aeronautical University, 600 South Clyde Morris Blvd., Daytona Beach, FL 32114, USA⁵ Department of Astronomy, Boston University, 725 Commonwealth Avenue, Boston, MA 02215, USA[†] This publication is partially based on observations obtained with the Apache Point Observatory 3.5-meter telescope, which is owned and operated by the Astrophysical Research Consortium.

M dwarf binary systems selected from the Sloan Low-mass Wide Pairs of Kinematically Equivalent Stars catalog (SLoWPoKES; Dhital et al. 2010). With presumably the same age and metallicity and near-equal masses, these are nearly identical twins. In addition, these are wide (~ 600 – 15000 AU) binary systems in which both stellar components have evolved independently, without affecting each other’s activity (as observed in tighter systems, e.g. Meibom et al. 2007; Morgan et al. 2012).

In this paper, we seek to characterize the differences in activity and variability of $H\alpha$ emission of M dwarfs by examining $H\alpha$ activity over timescales of hours to days for these coeval twins. These binary M dwarfs are a unique test case for the relationships between mass, age, and activity. In Section 2, we describe the observations to select and characterize our active M dwarf sample in addition to our time-series spectroscopic observations of the active SLoWPoKES binaries. We describe the the individual $H\alpha$ light curves and variability trends in Section 3. In Section 4, we discuss our $H\alpha$ observations compared to the mean trends for large samples of M dwarfs.

2. OBSERVATIONS AND DATA REDUCTION

The SLoWPoKES catalog, constructed from the Sloan Digital Sky Survey (SDSS; York et al. 2000), comprises 1342 wide (≥ 500 AU) common proper motion pairs with at least one low-mass (K5 or later) component (Dhital et al. 2010). While these systems are classified as binaries based on common proper motion and distance alone, their probability of chance alignment is low. To be part of the SLoWPoKES catalog, each pair was required to have a false positive probability (calculated for each pair using a Galactic model including both stellar density and kinematics) of less than 5%. Dhital et al. (2012) obtained follow-up observations of a 111 of these pairs, finding that 87% showed good agreement in their radial velocities. The remaining 13% of those pairs were likely to be contaminated with low signal-to-noise observations of spectroscopic binaries (providing a challenge for the accurate measurement of radial velocities). As these common proper motion pairs have a high probability of being physically associated, we assume that they are wide binaries.

With a large number of binaries that extend down to $\sim M6$ spectral types, the SLoWPoKES catalog is an ideal source of coeval laboratories to conduct followup studies of M dwarfs. Because the SLoWPoKES binaries were identified from photometry and proper motions without spectroscopic information, the catalog does not include the magnetic activity as measured by $H\alpha$ emission for the component stars. Therefore, we selected an initial sample of SLoWPoKES binaries for spectroscopic observations. The components of the binaries were restricted to M0 and later dwarfs ($r - z \gtrsim 0.9$) and to have similar $r - z$ colors ($\Delta(r - z) \leq 0.25$), meaning the components are roughly within one-half spectral type. We also selected for well-resolved components that fit along the length of the slit (separations of 7 – $120''$) and a minimum brightness of $r \lesssim 18$. This resulted in 176 candidate pairs, 36 of which had been determined to be inactive by Dhital et al. (2012), giving an initial sample of 140 near-equal mass, M dwarf binaries. While this sample was chosen to be near-equal mass, there exists a small difference in their $r - z$ colors. Hereafter, we refer to the

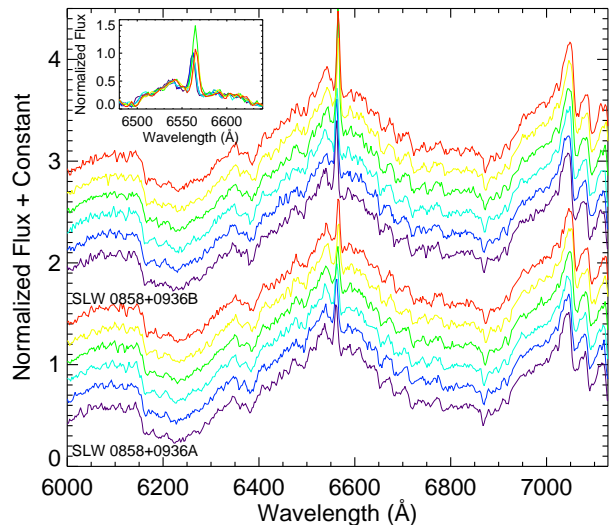


FIG. 1.— Red optical spectra (normalized flux as a function of wavelength) for the A and B components of SLW 0858+0936 during the time-resolved observations on UT 2011 Dec 29. Both the A component (bottom six spectra) and the B component (top six spectra) are shown at six different times ~ 1 hour apart, with time increasing from the bottom (purple) spectrum to the top (red) spectrum. The inset figure shows the $H\alpha$ emission from the B component; the green spectrum was taken during a flare.

component with the bluer $r - z$ color as the primary (A) and the one with the redder $r - z$ color as the secondary (B).

Out of the sample of 140 candidate SLoWPoKES binaries, we obtained optical ($\lambda \sim 5000$ – 10000 Å) spectra for 48 pairs (96 total stars) in our sample using the Dual Imaging Spectrograph (DIS) on the Astrophysical Research Consortium (ARC) 3.5-m telescope at Apache Point Observatory (APO). No selection criteria were initially applied, but brighter and redder systems were preferentially observed. The complete sample of observed M dwarf binaries is listed in Table 1. DIS uses a dichroic to split light into a red and a blue channel; for this study we only used the red channel. These data were taken with a $120''$ long, $1.5''$ wide slit, dispersed with the R300 (2.31 Å/pix) grating, resulting in an average resolution of $R \sim 1000$. Spectra for the components of a binary were obtained simultaneously by placing both targets on the spectroscopic slit. Figure 1 shows spectra of SLW 0858+0936 during time-resolved observations; those spectra are representative of typical spectra obtained during the observations. For each binary, we initially obtained 3 exposures of 1–10 min each to achieve a minimum total S/N of 20. Flats, biases, and HeNe-Ar comparison arcs were also taken at the beginning or end of every night. The data were bias subtracted, flat fielded, extracted, and wavelength calibrated (onto an air scale) using standard IRAF⁷ routines.

To identify a sample of $H\alpha$ -active M dwarf binaries for time-resolved observations, we first determined the spectral types by comparing each spectrum by eye with templates using the Hammer software (West et al. 2004;

⁷ IRAF is distributed by the National Optical Astronomy Observatories, which are operated by the Association of Universities for Research in Astronomy, Inc., under cooperative agreement with the National Science Foundation

Covey et al. 2007). In five cases, the spectral type of the A component was one subtype later than that of the B component, in contrast with their $r - z$ colors. We did not reassign types for these systems because of the uncertainties associated with spectral types; since our types are good to ~ 0.5 subtype, these types are still consistent with a slightly higher mass A component. We also used the Hammer to measure the H α equivalent width (EW; hereafter EW H α) for each component. The H α line region is defined as 6557.61–6571.61 Å, and the continuum regions are 6500–6550 Å and 6575–6625 Å. The Hammer applies a multi-part criteria to determine the activity of each object (described in detail by West et al. 2004). When considering spectra with S/N > 3 in the continuum region (a condition met by all our spectra), those with EW H α > 0.75 Å are considered active (y in Table 1), those with EW H α < 0.75 Å and an EW greater than 3 times its uncertainty are considered weakly active (w in Table 1), and those with EW H α below 3 times its uncertainty are considered inactive (n in Table 1). While the resolution of these spectra is somewhat lower than those taken by SDSS (R \sim 1000 compared to R \sim 2000) our H α EW measurements should be comparable to those performed on SDSS data.

Nineteen of the 96 stars exhibited H α in emission. Of the 48 binaries observed, eight exhibited H α emission in both components, and three exhibited H α emission in one component. In addition to measuring EW H α , we also calculated the spectral type-independent measure of activity strength ($L_{\text{H}\alpha}/L_{\text{bol}}$) for the active dwarfs. The conversion from EW H α to $L_{\text{H}\alpha}/L_{\text{bol}}$ relies on the χ factor, calculated by West & Hawley (2008) as a function of $i - z$ color or spectral type. We adopted χ as a function of spectral type to calculate $L_{\text{H}\alpha}/L_{\text{bol}}$ for each object. Spectral types, EW H α , and $L_{\text{H}\alpha}/L_{\text{bol}}$ are given in Table 1.

We selected the five brightest of the eight binaries with two active components for time-resolved spectroscopy. These five systems were each observed for 1–5 hrs per night for a total of 47 hours over 11 nights. We used the same setup for the time-resolved observations as for the single epoch observations, with typical exposure times of 1–5 minutes for each system. The UT dates and hours observed are given in Table 2. Four of the systems were observed on three or four different nights while SLW 2315–0045 was only observed on one night. We measured EW H α using the Hammer for each spectrum; the H α variations are discussed for each pair in the next section.

3. CHARACTERIZING H α LIGHTCURVES

Our initial goal was to determine if observed differences in EW H α between the two stars in each binary were due to variability, e.g., two objects with the same mean EW H α would appear different in single epoch observations if their instantaneous measured values differed from the mean. The light curves from the time-resolved observations are shown in Figure 2. Our initial examination of the light curves revealed the presence of flares, so we identified and removed the flares before examining the quiescent light curves in more detail.

3.1. Removing Flares

TABLE 2
LOG FOR TIME-DOMAIN OBSERVATIONS

UT	Designation	Total t_{obs} (hrs)	# flares	
			A	B
2011 Feb 18	SLW 0741+1955AB	0.31	0	0
2011 Mar 09	SLW 0858+0936AB	4.48	0	1
2011 May 02	SLW 1120+2046AB	3.80	0	0
2011 Aug 27	SLW 2315–0045AB	1.03	0	0
	SLW 0149+2215AB	0.07	0	0
2011 Oct 15	SLW 0149+2215AB	3.40	0	1
2011 Oct 24	SLW 0741+1955AB	0.80	0	0
	SLW 0149+2215AB	3.83	0	0
2011 Nov 28	SLW 0741+1936AB	5.20	0	1
2011 Dec 29	SLW 0858+0936AB	5.53	0	1
2012 Feb 16	SLW 1120+2046AB	4.73	0	0
2012 Feb 21	SLW 1120+2046AB	2.30	0	0
2012 Mar 14	SLW 1120+2046AB	6.92	0	1
2012 Mar 24	SLW 0858+0936AB	3.34	0	0
	SLW 0741+1936AB	1.37	0	0

TABLE 3
BINARIES WITH TIME-DOMAIN SPECTRA

Designation	Comp	Including Flares		Excluding Flares	
		$\langle \text{EW H}\alpha \rangle$	$\frac{\sigma_{\text{EW H}\alpha}}{\langle \text{EW H}\alpha \rangle}$	$\langle \text{EW H}\alpha \rangle$	$\frac{\sigma_{\text{EW H}\alpha}}{\langle \text{EW H}\alpha \rangle}$
SLW+		(Å)		(Å)	
0149+2215	A	2.17 ± 0.30	0.14	2.17 ± 0.30	0.14
	B	4.56 ± 1.43	0.31	4.10 ± 1.13	0.27
0741+1955	A	1.95 ± 0.57	0.30	1.47 ± 0.26	0.18
	B	5.25 ± 0.80	0.15	4.86 ± 0.43	0.09
0858+0936	A	2.66 ± 0.39	0.15	2.66 ± 0.39	0.15
	B	4.90 ± 2.07	0.42	4.35 ± 0.84	0.19
1120+2046	A	1.65 ± 0.74	0.45	1.65 ± 0.74	0.45
	B	5.49 ± 0.91	0.17	5.24 ± 0.54	0.10
2315–0045	A	3.96 ± 0.31	0.08	3.96 ± 0.31	0.08
	B	4.01 ± 0.26	0.07	4.01 ± 0.26	0.07

Both flares and quiescent activity are caused by the interaction of strong surface magnetic fields with the stellar atmosphere, but the details of that interaction are likely to be different. Flares are thought to be triggered by magnetic reconnection events resulting in dramatic heating over short timescales (e.g., Cram & Mullan 1979), while quiescent activity is characterized by emission over longer timescales from lower temperature material (e.g., Robinson et al. 1990). Our primary focus is the quiescent variability, but H α emission traces both quiescent emission and flares. We calculated the mean ($\langle \text{EW H}\alpha \rangle$) and standard deviation (σ_{EW}) of the H α emission both from the entire light curves and from the light curves with flares removed. While flares have been traditionally identified “by eye” (e.g., Pettersen et al. 1984), to clearly separate flares from smaller-scale variations we chose to remove flares using the quantitative method developed by Hilton (2011), which we summarize here.

We first determined a quiescent mean and standard deviation EW H α for each binary component on each night of data. For stars that appeared to exhibit a flaring event, we used the quiescent period before and/or after the flare to obtain our $\langle \text{EW H}\alpha \rangle$ and σ_{EW} . We then defined a flare as an event with at least one point above 3σ and at least five points above 2σ of the quiescent $\langle \text{EW H}\alpha \rangle$. Figure 3 shows a subset of the EW H α measurements of SLW 0858+0936AB (from UT 2011 Dec 29) with the quiescent mean as well as the 1σ and 2σ deviations given as dashed lines. The A component shows

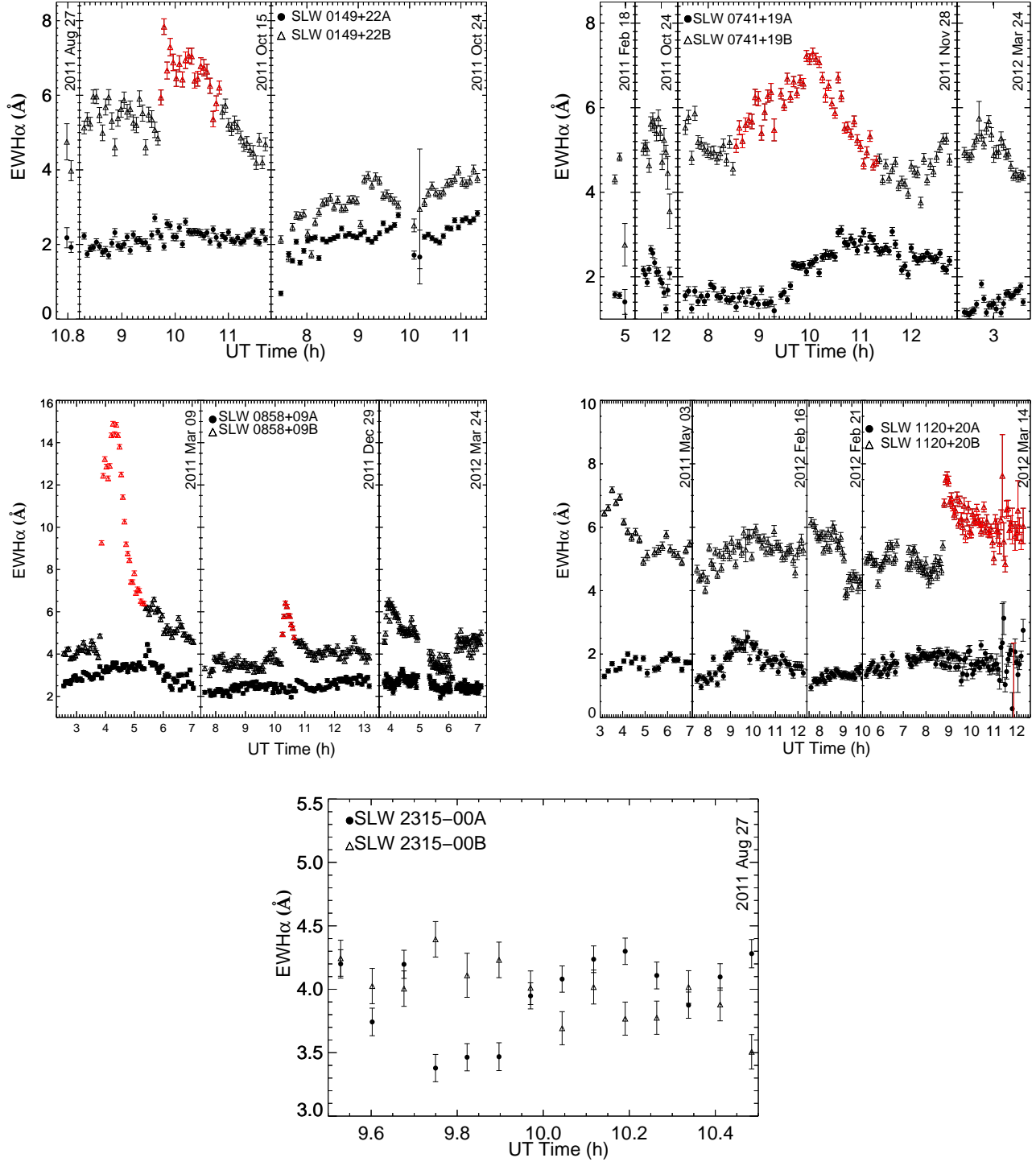


FIG. 2.— EW H α as a function of time for each of the binaries. (upper left): SLW 0149+22, (upper right): SLW 0741+19, (middle left): SLW 0858+09, (middle right): SLW 1120+20, (bottom): SLW 2315-00. Each panel is labeled with the UT dates when the binary was observed. The B component data are shown as open circles and the A component data are filled circles. The red data indicate the portion of the curve that has been classified as a flare event, as described in Section 3.1. Formal uncertainties are shown on each point; many are approximately the size of the point. These stars have separations far greater than those of interacting binaries, so any variations that are similar between the two stars are either coincidental or due to observational effects (e.g., changing airmass).

variations, but none are large enough to meet the flare criteria. The B component also varies throughout the night, with one of the variations being large enough to be considered a flare.

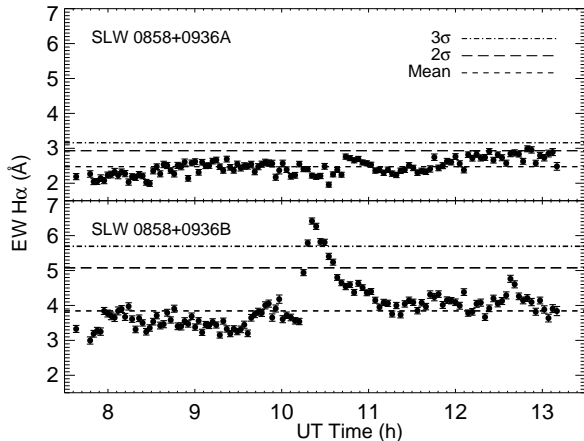


FIG. 3.— EW H α as a function of time for SLW 0858+0936A (top) and SLW 0858+0936B (bottom) on UT 2011 Dec 29. The data (black filled circles with error bars) are shown along with the mean and multiples of the standard deviation (dashed lines). According to the flare criteria described in Section 3.1, the A component shows only quiescent variations while the B component flares at $t = 10.3$ hr.

Using these criteria, we initially identified six flares. We then confirmed each flare by eye, accepting five flares and rejecting one spurious flare (on SLW 0741+19B; see discussion below), resulting in a total of five flares out of 47 hours of monitoring of the five binary systems (comparable to 94 hours on single M dwarfs). All five of the flares occurred on the B components of the binaries, including two on SLW 0858+09B. The number of flares on each star on each night is noted in Table 2 and the flares are indicated in the lightcurves shown in Figure 2.

3.2. EW H α Light Curves

The EW H α light curves shown in Figure 2 are described in detail below. The $\langle \text{EW H}\alpha \rangle$ and σ_{EW} were calculated both with and without flares and are given in Table 3. Here we discuss the properties with flares removed.

SLW 0149+2215: A total of 7.3 hours of data were obtained for this system over the course of three nights. The A component maintained a relatively constant EW H α of $\langle \text{EW H}\alpha \rangle = 2.17$ Å with $\sigma_{\text{EW}} = 0.30$ Å. H α emission from the B component was more variable, showing a 2 Å variation between the two longer nights of observations with $\langle \text{EW H}\alpha \rangle = 4.56$ Å and $\sigma_{\text{EW}} = 1.43$ Å. It is unclear whether the base value surrounding the flare on UT 2011 Oct 15 is true quiescence or part of a longer trend of elevated activity, but it is clear that the B component has stronger and more variable H α emission than the A component.

SLW 0741+1955: We observed this system for 7.7 total hours on four different nights. The emission from A component was relatively constant with an $\langle \text{EW H}\alpha \rangle = 1.95$ Å and $\sigma_{\text{EW}} = 0.57$ Å. The emission from the B component was both stronger ($\langle \text{EW H}\alpha \rangle = 5.25$ Å) and

more variable ($\sigma_{\text{EW}} = 0.80$ Å) than the A component. The emission from the B component included a flare, while the emission from the A component did not. At $t = 9.8$ hr, the A component showed an increase that was initially marked as a flare, but it was rejected when reviewed by eye because it lacked a decay phase after the initial rise.

SLW 0858+0936: This system was observed for 13.4 hours on three separate nights. The H α emission from the A component was relatively strong ($\langle \text{EW H}\alpha \rangle = 2.66$ Å) but not variable ($\sigma_{\text{EW}} = 0.39$ Å). The H α emission from the B component was very strong and variable ($\langle \text{EW H}\alpha \rangle = 4.90$ Å; $\sigma_{\text{EW}} = 2.07$ Å) even with the two flares excluded. On UT 2011 Mar 9, the H α emission showed a large flare that peaked at EW H $\alpha = 15$ Å and on UT 2011 Dec 29, a small flare peaked at an EW of H $\alpha = 6$ Å.

SLW 1120+2046: This binary was observed for a total of 17.8 hours during four nights. The H α emission from the A component was the weakest of all the observed M dwarfs ($\langle \text{EW H}\alpha \rangle = 1.65$ Å) but more variable than other A components ($\sigma_{\text{EW}} = 0.74$ Å). The mean H α emission from the B component was stronger than that of other B components ($\langle \text{EW H}\alpha \rangle = 5.24$ Å) with relatively low variability ($\sigma_{\text{EW}} = 0.54$ Å; similar to SLW 0741+19B). On the last night of observations for this pair, we observed a small flare on the B component which peaked at EW H $\alpha \sim 8$ Å.

SLW 2315–0045: This binary pair was both the latest-type dM in our sample (M5/M5) and has the least observations (one hour on a single night). This binary had the smallest difference in strength and variability between the two components, with values of $\langle \text{EW H}\alpha \rangle \sim 4$ Å and $\sigma_{\text{EW}} \sim 0.3$ Å for both A and B. During the short duration of our observations, SLW 2310–0045 was less variable than the other observed systems.

3.3. Variability

The production of H α emission by an active chromosphere is a dynamic process on timescales of minutes to decades. Several groups have used different statistics to characterize that variability; the ratio of maximum to minimum EW H α (Kruse et al. 2010; Lee et al. 2010), the standard deviation of EW H α (Gizis et al. 2002) and normalized standard deviation of EW H α (Bell et al. 2012). We choose to characterize variability with the standard deviation of EW H α ($\sigma_{\text{EW H}\alpha}$) and normalized variability with $\sigma_{\text{EW H}\alpha} / \langle \text{EW H}\alpha \rangle$ divided by $\langle \text{EW H}\alpha \rangle$. Table 3 includes these quantities for each of the twins with time-resolved data, and they are shown with respect to mean EW H α and $r - z$ color in Figure 4. The $\sigma_{\text{EW H}\alpha}$ and $\sigma_{\text{EW H}\alpha} / \langle \text{EW H}\alpha \rangle$ are slightly higher than the mean values reported by Bell et al. (2012) for M dwarfs with similar spectral types and emission levels, which could be due to the differences in cadence and timescale of the observations.

The un-normalized variability is on average higher for the B component than the A component. This is, perhaps, simply due to the B components having stronger activity than their twins. More H α emission allows a larger dynamic range for variation. Increasing variability with larger $\langle \text{EW H}\alpha \rangle$ is not visible when the normal-

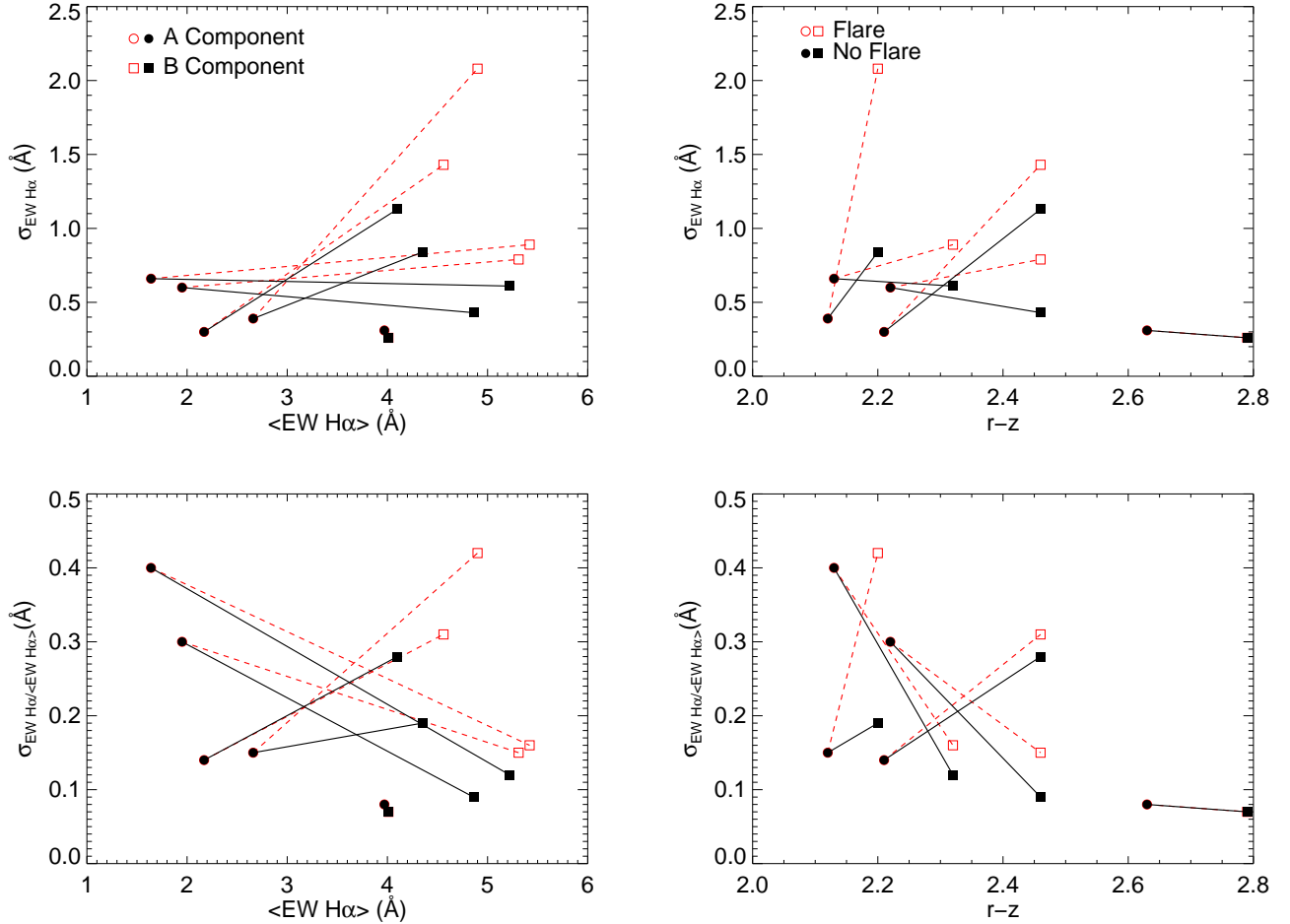


FIG. 4.— Variability of the twins with time resolved observations. The top two panels show the variability of EW H α ($\sigma_{\text{EW H}\alpha}$) as a function of the mean EW H α ($\langle \text{EW H}\alpha \rangle$; top left panel) and $r - z$ color (top right panel). The bottom two panels show the normalized variability of EW H α ($\sigma_{\text{EW H}\alpha} / \langle \text{EW H}\alpha \rangle$) as a function of the mean EW H α ($\langle \text{EW H}\alpha \rangle$; bottom left panel) and $r - z$ color (bottom right panel). Each A (circles) and B (squares) component is connected, and values computed with flares (open red symbols) are distinguished from values computed without flares (solid black symbols).

ized variability is instead examined. The four pairs with strong variability are evenly divided between the A and B components showing stronger variability. If variability was a strong function of age, we would expect the co-eval companions to have similar variability, but our sample reveals no relationship between age, activity level, and variability. If there are correlations between these quantities, larger samples of M dwarfs or longer timescale H α monitoring may be needed to detect them.

4. M DWARFS ACTIVITY TRENDS WITH MASS AND AGE

Comparing the H α emission of the A and B components to overall trends can provide unique constraints on the relationship between M dwarf mass, age, and activity. Figure 5 shows the activity strength ($L_{\text{H}\alpha} / L_{\text{bol}}$) of the active M dwarfs from West et al. (2011) as a function of $r - z$ color (often a proxy for spectral type; Bochanski et al. 2011). As expected, the activity strength declines slowly with decreasing mass (redder $r - z$ color) for these mid-M dwarfs (Hawley et al. 1996; Gizis et al. 2002; West et al. 2008, 2011), though with relatively large scatter: between $1.5 < r - z < 3.0$, there is at least an order of magnitude range of activity strengths ($L_{\text{H}\alpha} / L_{\text{bol}} \sim 0.0001$ to 0.001). We also show

the activity strength of the eleven binaries with at least one active component (including upper limits for the inactive component in those pairs). Of the eleven binaries, four have a more active A component, while the rest have more active B components. The binaries pairs do not, on average, follow the ensemble trend of decreasing activity strength with redder $r - z$ color.

To understand the significance of the differences between the A and B components compared to the scatter in emission strength for the ensemble of measurements, in Figure 6 we show the percent difference between the A and B components' $L_{\text{H}\alpha} / L_{\text{bol}}$ as a function of the A component's $L_{\text{H}\alpha} / L_{\text{bol}}$ compared to the normalized standard deviation of $L_{\text{H}\alpha} / L_{\text{bol}}$ values from Bell et al. (2012). If magnetic activity monotonically decayed for both A and B twin stars together, we would naively expect all active pairs to have a difference close to zero on the vertical axis. However, this zero difference only falls within the uncertainties of one system. This is true even of the five pairs with dedicated monitoring; the variability over timescales of hours to months does not bring the A and B emission strengths closer together. While no clear trend is seen as a function of the A component's $L_{\text{H}\alpha} / L_{\text{bol}}$, the

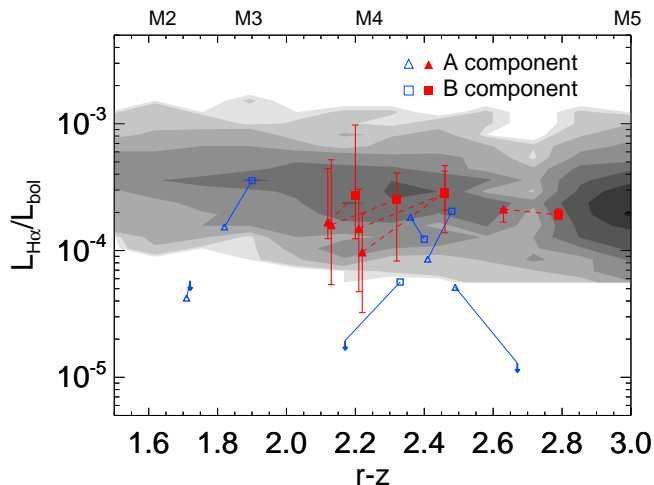


FIG. 5.— The ratio of the H α luminosity to the bolometric luminosity as a function of $r - z$ color for the active binaries in our sample. The distribution of active SDSS M dwarfs is also shown for comparison (contours; Bell et al. 2012). A (triangle) and B (square) components of each pair are connected (solid and dashed lines). For stars with single epoch data (blue), the measured $L_{H\alpha}/L_{bol}$ is shown while for pairs with time-resolved data (red), both the median and total spread in $L_{H\alpha}/L_{bol}$ are shown. For the three pairs consisting of one active and one inactive component, the upper limit of H α emission (the measured EW from the highest individual spectrum, which was not high enough to meet our criteria for active) is shown as a down arrow.

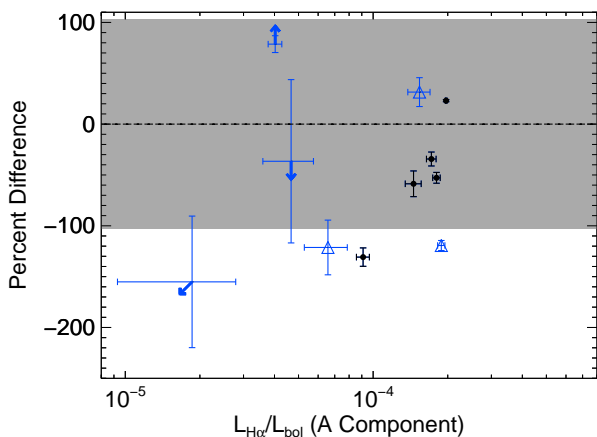


FIG. 6.— The percent difference in activity strength between A and B components for each pair as a function of the A component activity strength. Here, systems with a positive percent difference have stronger activity in the A component. Binaries with time-resolved observations (black circles) are distinguished from those with only a single set of observations (blue triangles). Systems with only one active component are represented with arrows denoting upper or lower limits; for SLW1446+5324, the limit is on both the A component H α and the difference between the A and B component. For comparison, the normalized standard deviation of the ensemble activity level for the M0-M5 dwarfs from Bell et al. (2012) is shown (grey shaded region). Systems falling outside the grey shaded region have significantly different levels of activity compared to the typical range of the ensemble.

difference in activity spans from -160 to 80% , with the majority of systems having stronger H α emission in the slightly redder B component.

Additionally, four of the pairs in our sample show differences in their activity significantly greater than the typical scatter from Bell et al. (2012), all in which the B

component has stronger activity. These are particularly interesting systems that would benefit from additional observations. It is possible that despite their coevality, these twin M dwarfs have different rotation rates and magnetic field strengths. Another possibility is the existence of Solar-like activity cycles that could be revealed through additional H α monitoring.

While there is not evidence for a strong trend between activity and age, our data are consistent with the “activity lifetime” model of M dwarf H α emission. Our full sample included 37 inactive pairs, three pairs with one active component and eight pairs with two active components. The 37 systems with two inactive components may be older than the active lifetimes for their spectral types. Based on the West et al. (2008) age-activity relations, this places lower limits on the stellar ages of ~ 1 Gyr for M0–M2 dwarfs, and 2–7 Gyr for M3–M5 dwarfs, which are typical of disk stars.

In the three binary systems from our sample for which only one stellar component showed H α activity, the active components (two A components and one B component) had relatively weak H α emission ($EW < 0.5\text{\AA}$). Given the moderate S/N and low spectral resolution of our observations, very weak emission from the “inactive” components may have been below our measurement sensitivity. These systems may be in fact be undergoing the transition from active to inactive states. This would in turn imply that the binary’s age is approximately at the expected activity lifetime (e.g., ~ 4 Gyr for M4). The relative scarcity of these systems in our dataset indicates that this transition must occur relatively quickly.

Variability may instead be a cause of the scatter in activity strength with respect to mass and age. If variability is the main cause for the scatter, we would expect the activity of all mid-M dwarfs to be about equal when observed over long timescales. For the binaries with time-resolved data, we plot the median value and the full range of observed activity strengths in Figure 6. These ranges show the possible range of values that would be observed for each M dwarf in a single spectrum. This variability ranges from a factor of two to an order of magnitude and is comparable to the full range of scatter in the single-epoch data, indicating that variability could be the main cause for the scatter. Variability does not, however, explain the differences between the A and B components because they persist on timescales of weeks to years. To understand the different H α strengths of coeval binaries, additional observations are needed.

5. SUMMARY

We presented optical spectra for 96 early- to mid-M dwarfs found in 48 coeval twin binary systems. Of those binaries, eight had H α emission from both components and three showed H α emission from one component. The active wide binary components did not show the similar levels of H α emission that would initially be expected from M dwarfs of the same mass and age. Instead, the A and B components exhibited different levels of emission, with four of the eleven having differences larger than the standard deviation of the scatter in $L_{H\alpha}/L_{bol}$ for the West et al. (2011) M dwarfs. Despite the mean trend of decreasing activity strength with decreasing mass, we found that seven of the eleven binaries had stronger activity on the less massive (B) component.

We also presented 47 hours spectroscopic monitoring for five of the wide binaries. We examined their H α light curves in detail, identifying five flares that all occurred on the B components of the binaries. The majority of these M dwarfs exhibited significant variability; the range of activity strength was comparable to the scatter in $L_{\text{H}\alpha}/L_{\text{bol}}$ as a function of $r - z$ color. Over the ~ 1 year timescale of the time-resolved observations, the observed binaries continued exhibit stronger activity from their B components, but variations on longer timescales (e.g., decades) may further modify their relative activity strengths. The variability from our time-resolved data showed no trends with either $r - z$ color or H α EW; we find that variability is independent of both stellar mass and activity strength.

While M dwarf ensemble trends indicate strong relationships between mass, age, and the presence and strength of activity, our observations reveal a complicated relationship between mass, age, and activity for individual stars. The differences in activity in coeval twins could indicate long timescale Solar-type variations in the magnetic field strength or could be due to intrinsic differences in rotation rate and magnetic field generation. Time-resolved observations over longer timescales, in addition to more detailed studies of coeval twins, will be instrumental in a complete understanding of M dwarf activity.

J. R. A. D. acknowledges funding from NASA ADP grant NNX09AC77G. S. D. acknowledges funding from NSF grant AST-0909463. A. A. W. acknowledges fund-

ing from NSF grants AST-1109273 and AST-1255568 and also the support of the Research Corporation for Science Advancement's Cottrell Scholarship.

Our work relies on data from the Sloan Digital Sky Survey. Funding for the SDSS and SDSS-II has been provided by the Alfred P. Sloan Foundation, the Participating Institutions, the National Science Foundation, the U.S. Department of Energy, the National Aeronautics and Space Administration, the Japanese Monbukagakusho, the Max Planck Society, and the Higher Education Funding Council for England. The SDSS Web Site is <http://www.sdss.org/>.

The SDSS is managed by the Astrophysical Research Consortium for the Participating Institutions. The Participating Institutions are the American Museum of Natural History, Astrophysical Institute Potsdam, University of Basel, University of Cambridge, Case Western Reserve University, University of Chicago, Drexel University, Fermilab, the Institute for Advanced Study, the Japan Participation Group, Johns Hopkins University, the Joint Institute for Nuclear Astrophysics, the Kavli Institute for Particle Astrophysics and Cosmology, the Korean Scientist Group, the Chinese Academy of Sciences (LAMOST), Los Alamos National Laboratory, the Max-Planck-Institute for Astronomy (MPIA), the Max-Planck-Institute for Astrophysics (MPA), New Mexico State University, Ohio State University, University of Pittsburgh, University of Portsmouth, Princeton University, the United States Naval Observatory, and the University of Washington.

REFERENCES

- Bell, K. J. et al. 2012, *PASP*, 124, 14
 Bochanski, J. J. et al. 2010, *AJ*, 139, 2679
 Bochanski, J. J., Hawley, S. L., & West, A. A. 2011, *AJ*, 141, 98
 Bopp, B. W. & Schmitz, M. 1978, *PASP*, 90, 531
 Browning, M. K., Miesch, M. S., Brun, A. S., & Toomre, J. 2006, *ApJ*, 648, L157
 Chabrier, G. & Baraffe, I. 1997, *A&A*, 327, 1039
 Covey, K. R. et al. 2007, *AJ*, 134, 2398
 Cram, L. E. & Mullan, D. J. 1979, *ApJ*, 234, 579
 Dhital, S., West, A. A., Stassun, K. G., & Bochanski, J. J. 2010, *AJ*, 139, 2566
 Dhital, S., West, A. A., Stassun, K. G., Bochanski, J. J., Massey, A. P., & Bastien, F. A. 2012, *AJ*, 143, 67
 Dobler, W., Stix, M., & Brandenburg, A. 2006, *ApJ*, 638, 336
 Gizis, J. E., Reid, I. N., & Hawley, S. L. 2002, *AJ*, 123, 3356
 Gomes da Silva, J. et al. 2011, *A&A*, 534, A30
 Hawley, S. L., Gizis, J. E., & Reid, I. N. 1996, *AJ*, 112, 2799
 Hilton, E. J. 2011, University of Washington
 Irwin, J. et al. 2011, *ApJ*, 727, 56
 Johns-Krull, C. M. & Valenti, J. A. 1996, *ApJ*, 459, L95
 Kruse, E. A. et al. 2010, *ApJ*, 722, 1352
 Lee, K.-G., Berger, E., & Knapp, G. R. 2010, *ApJ*, 708, 1482
 Meibom, S., Mathieu, R. D., & Stassun, K. G. 2007, *ApJ*, 665, L155
 Morgan, D. P. et al. 2012, *AJ*, 144, 93
 Pettersen, B. R., Coleman, L. A., & Evans, D. S. 1984, *ApJS*, 54, 375
 Robinson, R. D., Cram, L. E., & Giampapa, M. S. 1990, *ApJS*, 74, 891
 Valenti, J. A. & Johns-Krull, C. 2001, in *Astronomical Society of the Pacific Conference Series*, Vol. 248, *Magnetic Fields Across the Hertzsprung-Russell Diagram*, ed. G. Mathys, S. K. Solanki, & D. T. Wickramasinghe, 179
 West, A. A. & Hawley, S. L. 2008, *PASP*, 120, 1161
 West, A. A. et al. 2008, *AJ*, 135, 785
 West, A. A. et al. 2004, *AJ*, 128, 426
 West, A. A. et al. 2011, *AJ*, 141, 97
 York, D. G. et al. 2000, *AJ*, 120, 1579

TABLE 1
LIST OF ALL OBSERVED BINARIES

Designation	Comp	RA (h m s)	Dec ($^{\circ}$ ' ")	dist ^a (pc)	P_{false} (%)	SpT	EW H α (\AA)	$r - z$	$i - z$	$L_{\text{H}\alpha}/L_{\text{bol}}$ ($\times 10^{-4}$)	Active?
SLW 0149+2215 ^b	A	01 49 49.54	+22 15 44.8	79	0.05	M5	2.17 ± 0.30	2.21 ± 0.02	0.77 ± 0.02	1.49	y
	B	01 49 48.99	+22 16 00.5	70		M4	4.56 ± 1.43	2.46 ± 0.02	0.85 ± 0.02	2.81	y
SLW 0214-1039	A	02 14 54.08	-10 39 31.2	191	0.53	M4	-0.14 ± 0.08	1.89 ± 0.03	0.64 ± 0.03	...	n
	B	02 14 56.02	-10 39 36.9	189		M4	-0.10 ± 0.12	1.94 ± 0.03	0.65 ± 0.03	...	n
SLW 0248-0108	A	02 48 48.90	-01 08 12.4	142	0.14	M3	0.00 ± 0.07	1.63 ± 0.03	0.55 ± 0.03	...	n
	B	02 48 50.02	-01 08 17.7	139		M3	-0.09 ± 0.11	1.66 ± 0.03	0.56 ± 0.03	...	n
SLW 0258-0711	A	02 58 07.59	-07 11 06.5	236	0.83	M4	-0.24 ± 0.09	1.98 ± 0.01	0.70 ± 0.01	...	n
	B	02 58 04.73	-07 10 42.7	255		M4	-0.07 ± 0.12	1.99 ± 0.01	0.71 ± 0.01	...	n
SLW 0421+0626	A	04 21 10.53	+06 26 42.5	157	0.08	M3	0.06 ± 0.06	1.93 ± 0.01	0.66 ± 0.01	...	n

TABLE 1 — *Continued*

Designation	Comp	RA (h m s)	Dec ($^{\circ}$ ' ")	dist ^a (pc)	P _{false} (%)	SpT	EW H α (\AA)	$r - z$	$i - z$	$L_{\text{H}\alpha}/L_{\text{bol}}$ ($\times 10^{-4}$)	Active?
SLW 0450–0412	B	04 21 08.91	+06 27 00.7	144		M3	0.04 \pm 0.08	2.11 \pm 0.01	0.73 \pm 0.01	...	n
	A	04 50 10.52	–04 12 33.5	49	0.01	M3	0.14 \pm 0.06	2.07 \pm 0.02	0.71 \pm 0.02	...	n
	B	04 50 09.71	–04 12 29.6	51		M2	–0.02 \pm 0.10	2.18 \pm 0.02	0.74 \pm 0.03	...	n
SLW 0741+1955 ^b	A	07 41 55.34	+19 55 45.8	66	0.07	M4	1.95 \pm 0.57	2.22 \pm 0.01	0.79 \pm 0.01	0.97	y
	B	07 41 57.06	+19 55 33.2	78		M4	5.25 \pm 0.80	2.46 \pm 0.01	0.90 \pm 0.01	2.88	y
SLW 0756+4619	A	07 56 44.79	+46 19 57.2	134	0.09	M4	–0.23 \pm 0.06	1.91 \pm 0.02	0.64 \pm 0.02	...	n
	B	07 56 46.47	+46 19 46.8	136		M4	–0.19 \pm 0.06	1.93 \pm 0.02	0.65 \pm 0.02	...	n
SLW 0819+3206	A	08 19 47.08	+32 06 53.8	262	1.20	M4	–0.14 \pm 0.15	1.91 \pm 0.01	0.67 \pm 0.01	...	n
	B	08 19 46.57	+32 06 43.0	251		M3	0.07 \pm 0.14	1.94 \pm 0.01	0.67 \pm 0.01	...	n
SLW 0819+4731	A	08 19 21.00	+47 31 59.3	205	0.57	M2	–0.24 \pm 0.06	1.29 \pm 0.03	0.49 \pm 0.03	...	n
	B	08 19 26.10	+47 32 14.1	211		M2	–0.08 \pm 0.07	1.34 \pm 0.03	0.49 \pm 0.03	...	n
SLW 0835+3826	A	08 35 30.90	+38 26 12.4	117	0.23	M3	–0.15 \pm 0.06	1.84 \pm 0.03	0.64 \pm 0.03	...	n
	B	08 35 30.94	+38 26 30.8	117		M3	–0.14 \pm 0.07	1.88 \pm 0.03	0.64 \pm 0.03	...	n
SLW 0847+2539	A	08 47 48.94	+25 39 29.7	169	0.36	M3	0.01 \pm 0.07	1.62 \pm 0.01	0.55 \pm 0.01	...	n
	B	08 47 50.33	+25 39 34.2	166		M3	–0.05 \pm 0.08	1.66 \pm 0.01	0.57 \pm 0.01	...	n
SLW 0853+0325	A	08 53 58.87	+03 25 07.9	185	0.29	M3	–0.20 \pm 0.07	1.62 \pm 0.02	0.57 \pm 0.03	...	n
	B	08 54 01.31	+03 25 27.0	191		M3	0.14 \pm 0.07	1.66 \pm 0.02	0.58 \pm 0.03	...	n
SLW 0858+0936 ^b	A	08 58 57.80	+09 36 59.1	65	0.01	M4	2.66 \pm 0.39	2.12 \pm 0.02	0.72 \pm 0.02	1.67	y
	B	08 58 54.73	+09 37 23.7	63		M4	4.90 \pm 2.07	2.20 \pm 0.02	0.75 \pm 0.02	2.71	y
SLW 0919+2417	A	09 19 41.98	+24 17 10.5	173	0.41	M5	0.36 \pm 0.11	2.25 \pm 0.02	0.77 \pm 0.02	...	n
	B	09 19 42.49	+24 17 24.2	166		M5	–0.05 \pm 0.27	2.26 \pm 0.02	0.79 \pm 0.02	...	n
SLW 0934+1512	A	09 34 35.01	+15 12 41.8	128	0.13	M4	–0.41 \pm 0.06	2.05 \pm 0.02	0.70 \pm 0.02	...	n
	B	09 34 33.16	+15 12 58.9	138		M4	–0.39 \pm 0.08	2.09 \pm 0.02	0.73 \pm 0.02	...	n
SLW 0949+0404	A	09 49 17.24	+04 04 15.7	194	0.24	M4	–0.38 \pm 0.13	2.04 \pm 0.03	0.70 \pm 0.02	...	n
	B	09 49 15.94	+04 03 53.1	191		M4	–0.19 \pm 0.09	2.06 \pm 0.03	0.71 \pm 0.02	...	n
SLW 0951+3709	A	09 51 26.44	+37 09 55.0	144	0.32	M5	2.82 \pm 0.29	2.36 \pm 0.03	0.84 \pm 0.03	1.83	y
	B	09 51 24.91	+37 10 35.0	145		M5	1.89 \pm 0.27	2.40 \pm 0.03	0.83 \pm 0.03	1.23	y
SLW 0954+0647	A	09 54 06.37	+06 47 03.7	114	0.07	M3	2.37 \pm 0.08	1.82 \pm 0.02	0.65 \pm 0.02	1.54	y
	B	09 54 02.54	+06 45 49.7	111		M3	5.49 \pm 0.09	1.90 \pm 0.02	0.68 \pm 0.02	3.56	y
SLW 1022+1733	A	10 22 50.92	+17 33 14.3	203	0.35	M3	0.52 \pm 0.12	1.71 \pm 0.03	0.58 \pm 0.03	0.422	w
	B	10 22 51.50	+17 33 07.8	209		M3	–0.15 \pm 0.11	1.72 \pm 0.03	0.58 \pm 0.03	...	n
SLW 1032+3823	A	10 32 00.11	+38 23 33.4	152	0.23	M3	–0.22 \pm 0.07	2.10 \pm 0.02	0.76 \pm 0.03	...	n
	B	10 31 59.30	+38 23 37.1	138		M4	–0.12 \pm 0.12	2.21 \pm 0.02	0.81 \pm 0.03	...	n
SLW 1034+4040	A	10 34 15.27	+40 40 58.9	58	0.00	M3	–0.65 \pm 0.08	2.24 \pm 0.03	0.79 \pm 0.03	...	n
	B	10 34 09.33	+40 39 39.6	50		M3	–0.20 \pm 0.10	2.35 \pm 0.03	0.85 \pm 0.03	...	n
SLW 1036+0118	A	10 36 49.54	+01 18 51.2	147	0.12	M0	–0.30 \pm 0.10	1.14 \pm 0.02	0.40 \pm 0.03	...	n
	B	10 36 50.17	+01 19 04.8	155		M3	0.23 \pm 0.37	1.78 \pm 0.02	0.62 \pm 0.03	...	n
SLW 1120+2046 ^b	A	11 20 03.38	+20 46 53.2	96	0.06	M4	1.65 \pm 0.74	2.13 \pm 0.03	0.72 \pm 0.03	1.60	y
	B	11 20 05.26	+20 46 54.8	101		M4	5.49 \pm 0.91	2.32 \pm 0.03	0.80 \pm 0.03	2.52	y
SLW 1133+0035	A	11 33 36.99	+00 35 20.5	71	0.01	M4	–0.64 \pm 0.08	2.23 \pm 0.02	0.80 \pm 0.01	...	n
	B	11 33 37.48	+00 35 14.6	70		M4	–0.43 \pm 0.09	2.30 \pm 0.02	0.83 \pm 0.01	...	n
SLW 1204+1951	A	12 04 36.35	+19 51 34.6	66	0.02	M5	–0.47 \pm 0.06	2.72 \pm 0.01	0.95 \pm 0.02	...	n
	B	12 04 35.97	+19 51 47.6	75		M5	–0.75 \pm 0.10	2.89 \pm 0.01	1.01 \pm 0.02	...	n
SLW 1239–0305	A	12 39 21.63	–03 05 57.3	102	0.12	M4	1.32 \pm 0.26	2.41 \pm 0.02	0.88 \pm 0.01	0.857	y
	B	12 39 20.76	–03 07 30.5	113		M4	3.14 \pm 0.26	2.48 \pm 0.01	0.91 \pm 0.01	2.04	y
SLW 1241+4645	A	12 41 00.45	+46 45 29.1	267	1.48	M0	–0.43 \pm 0.06	1.07 \pm 0.02	0.37 \pm 0.02	...	n
	B	12 40 59.75	+46 45 09.9	294		M2	–0.15 \pm 0.12	1.42 \pm 0.02	0.50 \pm 0.02	...	n
SLW 1348+0811	A	13 48 02.47	+08 11 40.2	125	0.16	M2	–0.22 \pm 0.08	1.76 \pm 0.02	0.63 \pm 0.02	...	n
	B	13 48 00.48	+08 12 31.1	121		M3	0.11 \pm 0.10	1.92 \pm 0.02	0.67 \pm 0.02	...	n
SLW 1408+1130	A	14 08 54.13	+11 30 45.0	133	0.15	M3	–0.28 \pm 0.07	1.91 \pm 0.03	0.63 \pm 0.03	...	n
	B	14 08 49.87	+11 30 22.3	146		M3	–0.22 \pm 0.14	2.09 \pm 0.03	0.71 \pm 0.03	...	n
SLW 1441+0156	A	14 41 26.23	+01 56 02.0	94	0.31	M4	–0.40 \pm 0.06	2.29 \pm 0.03	0.81 \pm 0.03	...	n
	B	14 41 27.55	+01 56 16.4	80		M4	–0.33 \pm 0.10	2.49 \pm 0.03	0.89 \pm 0.03	...	n
SLW 1446+5324	A	14 46 55.22	+53 24 22.5	86	0.13	M4	–0.16 \pm 0.07	2.17 \pm 0.03	0.78 \pm 0.03	...	n
	B	14 46 55.57	+53 25 17.3	96		M4	0.87 \pm 0.14	2.33 \pm 0.03	0.84 \pm 0.03	0.195	w
SLW 1502+6057	A	15 02 01.04	+60 57 11.0	151	0.34	M2	0.01 \pm 0.06	1.52 \pm 0.02	0.52 \pm 0.02	...	n
	B	15 01 59.85	+60 57 36.3	151		M2	–0.14 \pm 0.07	1.53 \pm 0.02	0.52 \pm 0.02	...	n
SLW 1545+1859	A	15 45 35.39	+18 59 29.4	75	0.08	M4	–0.10 \pm 0.05	2.48 \pm 0.03	0.90 \pm 0.02	...	n
	B	15 45 34.62	+18 59 33.1	85		M5	0.06 \pm 0.08	2.67 \pm 0.03	0.98 \pm 0.02	...	n
SLW 1546+3928	A	15 46 54.08	+39 28 17.0	202	0.83	M2	0.03 \pm 0.16	1.65 \pm 0.03	0.64 \pm 0.03	...	n
	B	15 46 55.89	+39 28 07.8	229		M3	–0.12 \pm 0.25	1.76 \pm 0.03	0.67 \pm 0.03	...	n
SLW 1554+4425	A	15 54 04.02	+44 25 44.1	143	0.16	M2	–0.20 \pm 0.06	1.61 \pm 0.03	0.52 \pm 0.04	...	n
	B	15 54 03.81	+44 25 30.2	147		M3	–0.23 \pm 0.09	1.66 \pm 0.03	0.53 \pm 0.04	...	n
SLW 1914+7928	A	19 14 45.31	+79 28 49.5	305	4.15	M2	0.16 \pm 0.05	1.51 \pm 0.02	0.51 \pm 0.03	...	n
	B	19 14 48.26	+79 28 38.1	331		M2	–0.18 \pm 0.07	1.63 \pm 0.02	0.55 \pm 0.03	...	n
SLW 2112–0044	A	21 12 56.83	–00 44 45.4	324	1.03	M1	–0.15 \pm 0.07	1.27 \pm 0.01	0.47 \pm 0.01	...	n
	B	21 12 56.35	–00 44 57.5	323		M1	0.00 \pm 0.07	1.28 \pm 0.01	0.47 \pm 0.01	...	n
SLW 2208–0000	A	22 08 22.50	–00 00 33.3	163	0.56	M4	0.18 \pm 0.06	2.06 \pm 0.02	0.73 \pm 0.03	...	n
	B	22 08 23.00	–00 00 26.9	139		M4	0.20 \pm 0.10	2.12 \pm 0.02	0.74 \pm 0.03	...	n
SLW 2212+4015	A	22 12 31.82	+40 15 23.3	147	0.35	M4	–0.34 \pm 0.07	2.20 \pm 0.01	0.77 \pm 0.01	...	n
	B	22 12 34.81	+40 15 08.8	139		M4	–0.29 \pm 0.08	2.26 \pm 0.01	0.79 \pm 0.01	...	n
SLW 2244+2318	A	22 44 20.21	+23 18 04.4	91	0.06	M4	–0.42 \pm 0.07	2.29 \pm 0.02	0.82 \pm 0.02	...	n
	B	22 44 19.96	+23 18 13.6	84		M4	–0.47 \pm 0.08	2.31 \pm 0.02	0.84 \pm 0.02	...	n
SLW 2253+2726	A	22 53 03.55	+27 26 46.3	70	0.55	M5	0.79 \pm 0.05	2.49 \pm 0.02	0.87 \pm 0.03	0.513	w
	B	22 53 04.31	+27 26 54.1	67		M5	0.30 \pm 0.08	2.67 \pm 0.02	0.94 \pm 0.03	...	n

TABLE 1 — *Continued*

Designation	Comp	RA (h m s)	Dec ($^{\circ}$ ' ")	dist ^a (pc)	P_{false} (%)	SpT	EW H α (\AA)	$r - z$	$i - z$	$L_{H\alpha}/L_{bol}$ ($\times 10^{-4}$)	Active?
SLW 2254–0931	A	22 54 51.34	–09 31 29.5	112	0.22	M4	-0.25 ± 0.06	2.18 ± 0.02	0.75 ± 0.02	...	n
	B	22 54 53.89	–09 32 36.7	128		M5	-0.40 ± 0.12	2.32 ± 0.03	0.80 ± 0.04	...	n
SLW 2258+2806	A	22 58 58.20	+28 06 25.2	211	0.61	M5	0.04 ± 0.05	1.87 ± 0.02	0.64 ± 0.03	...	n
	B	22 58 56.47	+28 05 54.8	203		M4	0.20 ± 0.05	1.91 ± 0.02	0.66 ± 0.03	...	n
SLW 2309+2440	A	23 09 32.55	+24 40 25.9	177	0.42	M2	-0.07 ± 0.08	1.53 ± 0.03	0.55 ± 0.02	...	n
	B	23 09 32.26	+24 40 48.9	182		M2	0.08 ± 0.08	1.60 ± 0.03	0.56 ± 0.02	...	n
SLW 2310+2201	A	23 10 50.47	+22 01 24.6	175	0.31	M3	-0.15 ± 0.07	1.83 ± 0.02	0.64 ± 0.03	...	n
	B	23 10 51.90	+21 59 50.7	180		M3	-0.10 ± 0.09	1.95 ± 0.02	0.68 ± 0.03	...	n
SLW 2311+0802	A	23 11 24.12	+08 02 51.5	154	0.24	M5	0.32 ± 0.09	2.14 ± 0.02	0.74 ± 0.03	...	n
	B	23 11 23.53	+08 02 52.2	146		M5	0.35 ± 0.10	2.20 ± 0.02	0.76 ± 0.03	...	n
SLW 2315–0045 ^b	A	23 15 44.02	–00 45 00.6	50	0.01	M5	3.96 ± 0.31	2.63 ± 0.03	0.92 ± 0.03	2.12	y
	B	23 15 46.63	–00 44 06.2	51		M5	3.01 ± 0.26	2.79 ± 0.03	0.98 ± 0.03	1.91	y

^a Distances were calculated using the Bochanski et al. (2010) M_r as a function of $r - z$.^b For binaries with time-resolved observations, the mean and standard deviation of observations, with flares included, are listed for H α EW.